A Method for Modeling System Driven Uncertainty During Probabilistic Part Life Analyses

Jon M. Wallace*, Vitali Volovoi†, and Dimitri N. Mavris‡
Aerospace Systems Design Laboratory, Georgia Institute of Technology, Atlanta, GA, USA

Probabilistic part life analyses of turbine components have typically been conducted in an ad-hoc fashion with respect to the influence of the system. While this approach greatly simplifies the analysis, significant errors and misleading results are possible. However, directly modeling the system analyses in a fully probabilistic and integrated fashion can be prohibitive in terms of the infrastructure required.

An efficient approach to characterizing and quantifying the system-driven input for probabilistic part life assessments is proposed. The approach is demonstrated for a turbine blade operating in a medium size commercial transport jet. The results of this demonstration illustrate how the component parameters and failure mechanisms can be qualitatively identified and the complex probabilistic input modeled as driven by the system behavior.

I. Introduction

RELIABILITY, or probabilistic failure, assessments of turbine components can quickly become highly involved when considering the many contributing analyses at the component level. Unfortunately, this complexity is exacerbated when one considers the upstream contributing analyses that account for the system's influence on the component initial and boundary conditions. Reducing the dimensionality of this complex space is advantageous from a resource perspective. Therefore, analysts typically will determine a nominal set of local conditions from a system level analysis, parameterize the component specific variables, and perform analysis, design, and probabilistic studies using this component-centric viewpoint. However, relationships between the system and component intermediate parameters are often neglected. Hence, the question arises of whether or not this approach is adequate. Recent studies[8] have shown that this approach can introduce considerable error in component analysis activities, both from a qualitative and a quantitative perspective. An improved posture towards part probability assessments by considering the relationship between the part and the system in which it operates is merited. Conceptualizing and implementing such a posture is the focus of this study.

First, a qualitative approach based on system safety principles is prescribed that reflects the system top-level safety requirements and translates them to the component level. Decomposition and synthesis steps are then prescribed to process this raw information into a specific set of relevant failure modes, intermediate parameters, and parameter characteristics. As a result, the appropriate contributing analyses and engineering models can be selected and properly integrated. The next step in the prescribed methodology is the local statistical space assessment which involves querying the system in such a way that an efficient characterization and quantification of the system's non-deterministic influence can be ascertained. This unique procedure for accomplishing this step is demonstrated. Rather than describe the steps of this approach abstractly then repeat them for a given application, they are described as applied to a relevant industry problem: the probabilistic failure assessment of a gas turbine airfoil.

*Currently: Research Engineer, ExxonMobil Upstream Research Company, Houston, TX, and Member AIAA.
†Research Engineer, Member AIAA.
‡Associate Professor, Associate Fellow AIAA.

II. Turbine Blade Application

Conducting probabilistic propulsion system part failure assessments is a relevant industry problem as some critical turbine components experience considerable scatter in their actual service lives. Therefore, the problem pursued in this study is to efficiently, yet accurately provide an early assessment of the reliability of a gas turbine blade for a simplified cruise operating condition. This problem is of great importance to the aerospace and power generation industries as hot gas path turbine components exhibit considerable scatter in their useful life which can only partially be explained through inherent variation of the components properties. The remaining variation is attributed to the interaction between the component and the system within which it operates. Fittingly, a modeling and analysis environment is necessary which can permit the integration of sources of component failure uncertainty. A suitable multi-physics environment has been created to automate the failure assessment of the aircraft gas turbine airfoil as a function of material and system-induced variation.

III. Decomposition

First, the pertinent component properties and relationships to the system behavior must be identified. The initial step taken during decomposition is to assess the functional characteristics of the component relative to the system-level safety and reliability goals. Such a characterization for the turbine blade is shown in Figure 1. The dashed line around the process column is the selected control volume. This control volume serves as a boundary between the perimeter of the component and any medium which work is imposed to or from the component, depicted by the input column, for it to complete its process functions. In this case, high energy flow leaving the combustor strikes the turbine blade and by virtue of the aerodynamic shape of the blade some of this energy is converted into a resultant lift vector on the blade which results in a torque applied to the turbine rotor. Since the airfoil is exposed to exceedingly high temperatures, coolant flow at a much lower temperature is extracted from the compressor is pumped through the internal passages of the blade to assist in maintaining the blade metal temperature. The external fluid imposes work on the blade while the internal flow extracts heat. This results in the conversion of some of the core flow energy to shaft power to drive the compressor where the byproduct leaving the blade is both lower energy core flow and higher energy coolant flow. Another implied, yet no less important, function is to maintain the safety of the system. A failure of the component in terms of separation would likely result in a cascading and perhaps even a catastrophic failure of the system. Thus, the functional purpose of the turbine blade is to safely convert some of the high energy core flow into shaft power to drive the compressor.

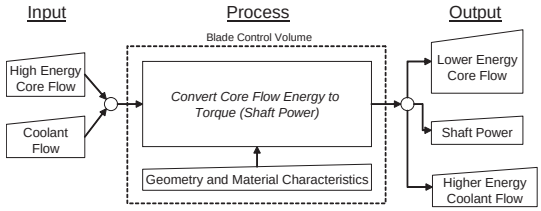

Figure 1. Blade Functional Relationship Diagram

Now that the driving functions of the blade have been identified the failure modes that could lead to a malfunction are to be determined. There are numerous potential failure modes of a second stage turbine blade. Three failure modes are considered for this study based on a previously completed study of a similar component under similar operating conditions[1,2,3]. They are *creep rupture*, because of the anticipated high operating temperature and stress; *fatigue* due to the high cyclic stress induced by the rotational speed of the rotor; and material strength *overstress* which is also driven by the rotor speed. These failure mechanisms are discussed further in the synthesis step described in section IV.

The mechanics involved with each of these failure modes is then inspected and related to the parameters identified through the functional relationship exercise (see Figure 1). A useful way to organize this information is given by Table 1. Each of the failure modes are list in the first columen and crossed with each of the component functions. Next, the various input parameters are organized into mass, energy, and characteristics categories and then cross listed with the various failure modes that they influence.

The information give by Table 1 can then be used to prescribe the appropriate modeling and simulation environment characteristics. For instance, all three failure modes require knowledge of the state of stress of the component so a mechanical analysis is required. Also, the creep rupture analysis as well as the required material model both require a prediction of the metal temperature distribution and thus a thermal solid analysis is required. Also, the parameters identified in Table 1 are further classified across several categories which provides additional insight to the conditions leading to the synthesis step of this approach.

Table 1. Blade Failure Mode Identification.

	Function		Parameters				
			Mass		Energy	Characteristics	
Failure Mode	Safety	Extract Energy	Core Flow	Coolant Flow	Rotor Speed	Geometry	Material
Creep	✓	✓	✓	✓	✓	✓	✓
Fatigue	✓	✓			✓	✓	✓
Overstress	✓	✓			✓	✓	✓

IV. Synthesis

Now that the failure posture of the blade has been assessed, an appropriate failure modelling and simulation environment is sought. Within this step, the actual analyses, their complementary assumptions, and flow of information between the system-level, intermediate, and failure analyses are defined and a baseline analysis performed.

A. System Model: Aircraft Jet Engine

The propulsion system selected for this study is a generic separate flow turbofan engine typical of those that power medium sized transport aircraft such as the B737 aircraft. Overall pressure and bypass ratios of the propulsion system are roughly 30:1 and 6:1, respectively. The maximum thrust at sea-level static conditions is around 20,000 lb_f. The vehicle mission used in this study is typical of a B737 aircraft; although, it has been simplified to facilitate the demonstration of the proposed method. Only the cruise condition is considered for this study. The take-off and landing segments are modelled as discontinuous jumps in engine rotor speed between the shut-down and cruise segments of the operating profile. The cruise segment occurs at an altitude of 35,000 feet and a speed of Mach 0.745 as expected for this type of aircraft. The operating parameters identified for this study are the cruise altitude and Mach number, and the change in ambient temperature.

A thermo-dynamic cycle analysis is used to represent the engine system. Analyzing the engine cycle provides system-driven aerothermal and mechanical input necessary for the subsequent component specific analyses. The thermodynamic cycle is implemented using a baseline NEPP model which calculates 1-D steady-state engine station and component properties for a given operating condition,[4,5] The thermodynamic cycle parameters identified for this study are given in Table 2. They include three operational parameters representing the cruise flight condition, altitude, Mach, and ambient temperature change, ΔT_a. The required output provided by the cycle analysis is the high-pressure rotor speed, RN, and turbine entrance and compressor exit temperatures, which are assigned as the blade coolant and external gas flow temperatures, T_c and T_g, respectively. Once these output parameters are calculated, they then become input to the component level analyses, solid, material, and failure models, discussed next.

B. Solid Model: Thermo-Mechanical Finite Element Analysis

The 2nd stage turbine bucket is a complex 3-D part. To determine the complex state of solid temperature, stress, and strain, a 3-D finite element mesh, shown in Figure **??**, was utilized. The finite element mesh consists of around 92,000 nodes and 75,000 elements. The calculation of the metal temperatures and mechanical stress requires a thermo-mechanical solid analysis. This analysis is conducted using ANSYS 5.7 FEA software. The baseline finite element model consists of the finite element mesh and thermal boundary conditions in the form of near-surface gas temperatures and heat transfer coefficient fields, shown in Figure

Table 2. Engine Cycle Parameters.

Parameter	Description	Class	Units	Mean	σ	Distribution
Altitude	–	Control	feet	35,000	1750	Normal
Mach	Flight Speed	Control	–	0.745	0.03725	Normal
ΔT_a	Ambient Temp. Change	Noise	$^\circ F$	0	15	Normal
T_c	Coolant Temp.	Response	$^\circ F$	–	–	–
T_g	Core Temp.	Response	$^\circ F$	–	–	–
RN	Rotor Speed	Response	rpm	–	–	–

2, mechanical boundary conditions in the form of the solid temperature distribution[a], inertial load in the form of a rotor speed specification, and displacement boundary conditions, shown in Figure 3 as well as temperature dependent material properties. See sub-section C for a description of the material properties

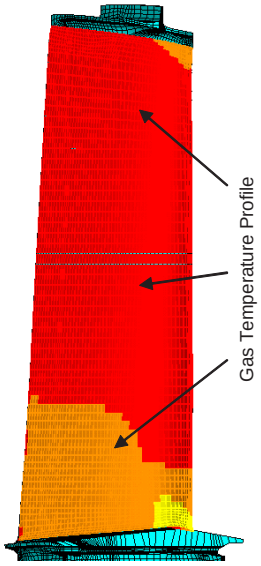

Figure 2. Thermal FEM Boundary Conditions

used in this study.

Although the thermal and mechanical analyses are in reality coupled, this study models them as uncoupled to maintain an acceptable computational run time. Therefore, a converged thermal analysis is found and the resulting solid temperature solution provided as a boundary condition input for the stress (mechanical) analysis. The result of the thermal solid analysis during each iteration as the thermal solution converges is a completely stabilized metal temperature distribution which is provided as input to the material analysis. The material analysis in turn provides an updated material thermal property matrix to the thermal solid analysis and the process repeated. Consequently, a coupling *is* created through this dual-analysis interaction resulting in a non-linear FEA solution. Once the converged thermal solid solution is found, a full stress and strain distribution is determined using the rotor speed and pressure distribution input from the cycle analysis, the metal temperature distribution from the thermal analysis, and the mechanical property matrix from the material analysis. These solid solutions are then provided as input to the failure mode analysis.

C. Material Model: Nimonic80A

The blade material selected for this study is the nickel-based alloy Nimonic80A. Room temperature physical, mechanical, strength, creep rupture, and fatigue properties used in this study are listed in Table 3. Values for these parameters for temperatures ranging from room temperature ($68^\circ F$) up to $1800^\circ F$ were used as input to the various analyses and are provided in reference.[6] In addition to the room temperature

[a]Solid temperature distribution is not shown in Figure 2.

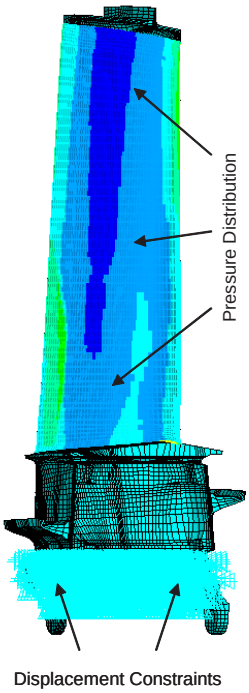

Figure 3. Mechanical FEM Boundary Conditions

values, representative statistical properties of these material parameters are given in Table 3. The statistical properties are the room temperature material property variations. Since statistical variation for higher temperatures was not available, it is assumed that the variation at any point along the temperature dependent material property curve has the same statistical variation as the room temperature variation.

Table 3. Blade Material Parameters.

Parameter	Description	Units	μ	σ	Distribution
EX	Elastic Modulus	psi	33E6	1.65E6	Normal[1]
NUXY	Poisson's Ratio	–	0.3	–	Constant
KXX	Thermal Conduct.	$\frac{Btu \cdot in}{sec \cdot ft^2 \cdot {}^\circ F}$	1.4898E-4	2.998E-6	Normal[2]
ALPX	Thermal Expansion	${}^\circ F \cdot 10^{-6}$	7.0$\overline{5}$E-6	1.4$\overline{1}$E-7	Normal[2]
CP	Specific Heat	$\frac{Btu}{lb \cdot {}^\circ F}$	41.3	–	Constant
DENS	Density	$\frac{lb}{g \cdot in^3}$	7.667E-4	1.533E-5	Normal[1]
CN	Creep Variation	–	0	1	Normal[2]
SY	Yield Strength	ksi	112	4.5	Normal[3]
SU	Ultimate Strength	ksi	180	7.2	Normal[3]
SFP	Fatigue Constant	ksi	327.05	6.2	Normal[4]
B	Fatigue Exponent	–	-0.117	0.01053	Normal[4]

[1]Sues et al.;[7] [2]Wallace and Mavris[8];[2] [3]Wu, Y.-T.[9]
[4]Pascual, F.G. and Meeker,W.Q.[10]

D. Failure Models: Creep Rupture and Fatigue

The material creep rupture life model used in this study is the Orr-Sherby-Dorn (OSD) three-term function based on the Arrhenius activation energy.[11] The OSD creep life function gives the elapsed time when the material reaches a specified creep strain limit given as

$$t_{creep} = e^{\frac{1}{A+B\log(\overline{\sigma})}+\frac{\frac{-Q}{R}}{T+459.67}+CN \cdot SE} \tag{1}$$

where $\overline{\sigma}$ is the equivalent stress (resolved during the cruise operating condition), T is the temperature, and the parameters A, B, and -Q/R are empirically determined creep constants corresponding to the time at

which the accrual of a pre-defined amount of creep strain is reached. The third term in the exponential represents the statistical variation of the creep rupture life, where CN is a standard normal variable and SE is a constant also determined empirically from test data. Several tests at various levels of stress and temperature must be performed to determine the creep-strain limit constants. They are unique both to the type of material used as well as the creep strain limit specified. Using equation (1) the creep life at each element can be determined as a function of several upstream variables such as bucket external and internal heat transfer boundary conditions, material properties, and geometry. Additional material characterization information for creep life modeling of nickel-based super alloys is given by Daleo et al.,[12,13].

The fatigue failure failure mode is more involved. Assuming that linear-elastic conditions exist, the straightforward stress-life, S-N, approach[14] can be utilized to estimate the number of cycles to failure given completely reversed, constant stress cycle amplitude. The following relationship is commonly used in the stress-life approach

$$\sigma_{ar} = \sigma_f^{'}(2N_f)^b \tag{2}$$

where $\sigma_f^{'}$ is the fatigue strength coefficient, N_f is the cycles to failure, and b is the fatigue exponent. The two fatigue constants, $\sigma_f^{'}$ and b, are found by fitting the following two constants to stress versus life results from coupon size test specimens, $C_1 = 2^b\sigma_f^{'}$ and $C_2 = b$. The fatigue life for a given level of stress would then be computed using

$$N_f = 0.5\left(\frac{\sigma_{ar}}{\sigma_f^{'}}\right)^b \tag{3}$$

where σ_{ar} is the equivalent completely reversed stress. This approach has been successfully applied to the case of tensile fatigue loading of ductile metals.[15]

At this point, it is necessary to make another simplifying assumption with regards to the fatigue analysis. The Morrow fatigue function assumes that the stress cycle amplitude is constant. Consequently, the stress cycle generated within the context of this problem is defined as the centrifugal stress cycling between the zero stress condition before starting the engine and the stress state at the cruise condition. Realistically, the stress-state is highly complex in a temporal sense as the engine operating conditions vary greatly over the mission profile of the vehicle. Further, material property and geometry non-linearity and perhaps even temporal randomness may also exist, which further complicate the analysis. *Consequently, the failure functions considered in this analysis are relatively straightforward and are assumed to be independent of each other.*

E. Baseline Failure Analysis Results

Up to this point, all of the necessary input and boundary conditions have been described and specified for the multi-response failure analysis of the 2^{nd} stage turbine bucket. Expected values for each of the random variables must then be chosen for the baseline case, and the entire analysis executed to determine the baseline failure solution. This process is depicted in Figure 4. First, system-level input (see Table 2) is provided to the system analysis module where the thermodynamic engine cycle analysis is run to determine the core flow gas temperature,X_{TC1}, cooling flow temperature, X_{TC2}, and turbine rotor speed. The turbine rotor speed is input to both the thermal and stress analysis modules denoted by X_{TC3} and X_{SC3}, respectively.

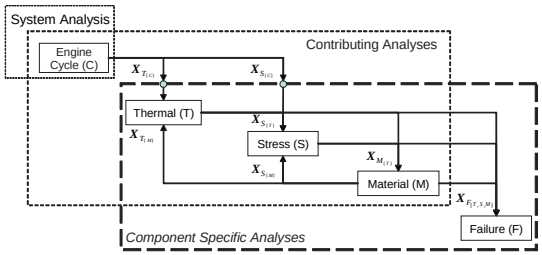

Figure 4. Blade Multi-Disciplinary Analysis Structure

The blade thermal analysis requires input from the cycle model, namely the core flow and coolant flow

temperatures ($X_{T_{C1}}$, $X_{T_{C2}}$) and rotor speed[b]($X_{T_{C3}}$), as well as from the material model which provides the thermal material properties ($X_{T_{M1}}$). The blade temperature distribution is determined during this step. Since the the thermal analysis is a function of the material properties and they are in turn a function of the metal temperature, a coupling scenario is created. The coupling is executed iteratively by the FEA analysis until a converged thermal solid solution is obtained. The baseline blade thermal solid solution using this process is shown by Figure 5. As expected based on previous blade analyses,[1] the hottest region of the blade is at the tip trailing edge and continues down a portion of the span of the trailing edge. The coolest region, intuitively, is near the base of the blade where the coolant flow is the coolest before much of the heat exchange along the inner cooling holes takes place[c].

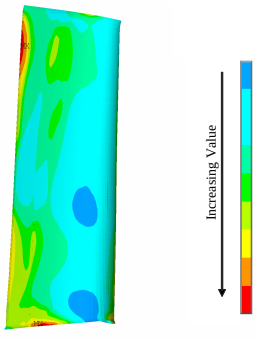

Figure 5. Baseline Thermal FEA Solution

A stress contour solution is then determined through the stress analysis step. Input for this step includes the engine rotor speed, $X_{S_{C3}}$, the metal temperature distribution from the thermal analysis, X_{S_T}, and the temperature dependent mechanical material properties, X_{S_M}, calculated using the converged temperature solution. The resulting equivalent stress contour is shown in Figure 6. Two high stress regions are found, around the mid-chord of the low pressure surface at the blade base and at the base of the leading edge. A high stress condition at the base of the blade is expected as the entire mass of the blade, and thus the blade centrifugal force, must be supported by this region. Likewise, less and less material has to be supported as you move outward along the span of the blade so the stress is lower in that direction. An exception is the somewhat oval-shaped low stress region located between the two high stress regions. Similar low stress regions are predicted near geometric stress concentration zones due to material equilibrium.

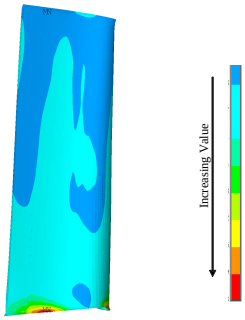

Figure 6. Baseline Mechanical FEA Solution (Equivalent Von Mises Stress)

Once the Mechanical analyis is complete and the stress distribution is determined, the failure analysis is then conducted. Input for the failure analysis includes the metal temperature distribution, X_{F_T}, the stress distribution, X_{F_S}, and temperature dependent material failure properties, X_{F_M}. The resulting stress solution is shown in Figure 6. The fatigue life solution, shown in Figure 7, follows a similar pattern. Low

[b]The heat transfer coefficient field boundary condition is actually a function of the rotational speed of the blade thus requiring the rotor speed as an input.

[c]The coolant flow enters the base of the blade, travels along the span of the blade in an outward radial direction, and exits the blade at its tip.

fatigue life regions, represented by the dark red zones, are coincident with the high stress regions shown in Figure 6 and a moderately low fatigue life region also appears near the lower trailing edge region away from the stress hot spots. In addition, a small but moderately low fatigue life region can be seen at the trailing edge tip region of the blade as well.

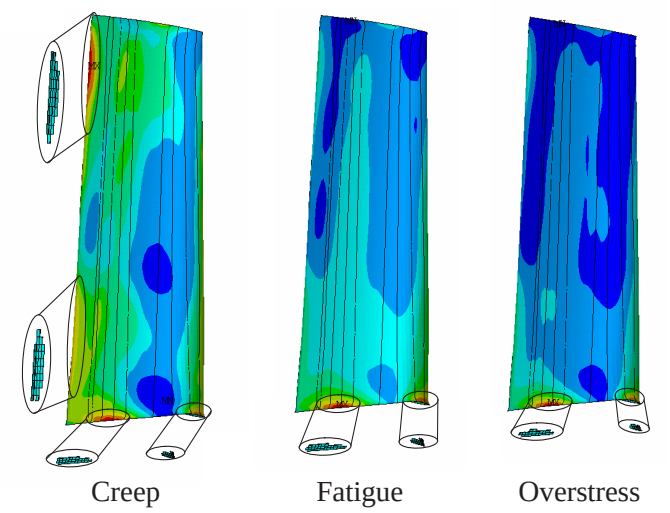

Figure 7. Identification of FEA Failure Hot Spots

The creep rupture solution requires input from all three upstream component-specific analyses. One would suspect that the limiting region of the blade due to creep rupture would be the thermal hot spot identified in Figure 5. However, several areas potentially limited by creep rupture are revealed as shown in Figure 7. Notice that creep limited regions are found at both of the high stress regions as well as the high temperature region of the blade. Further, moderate to severely limited regions span a much wider area of the blade such as the entire lower region of the blade trailing edge. The wide area covered by these limited creep rupture regions could complicate the adequate selection of hot spots as they may migrate across these regions for different values of the upstream blade analysis input.

V. Local Statistical Space Assessment

After the component analysis approach has been synthesized, the statistical input of the component must be determined. The upstream system level analyses are to be queried in such a way as to confidently, yet efficiently characterize and quantify the statistical properties of the local component analysis input. This information is important to several subsequent steps such as capturing possible joint randomness that may be present between the local input variables or deciding what range to consider for each local component analysis input parameter.

A. Baseline Monte Carlo Uncertainty Assessment

A cycle model Monte Carlo simulation using 100,000 samples was chosen and executed using the previously specified cycle model input parameter statistics given in Table 2. Statistical independence is assumed between each of the input parameters which are also assumed to be normal random variables. The statistics of the cycle model parameters are given in Table 4. These statistics suggest asymmetry, non-zero skewness, and positive kurtosis[d], $k > 3.0$, and therefore indicate that these response parameters are non-normal. Applying the Bera-Jarque hypothesis test of normality[16] quantifies this indication as the null hypothesis for normality is rejected for all three parameters. Finally, investigating the statistical behavior of these random parameters using probability plotting, shown in Figure 8, suggests that both the blade coolant and gas temperature

[d]The normal distribution is symmetric and therefore produces a skewness value of 0. The kurtosis of a normal distributed random variable is equal to three where values less than three and values greater than three indicate negative and positive kurtosis, respectively.

variables could be reasonably modeled by a normal distribution but are more likely to follow a lognormal distribution. However, the rotor speed follows more of a lognormal distribution rather than a normal one as the tail of the normal probability plot for the rotor speed data diverges considerably.

Table 4. Cycle Model Baseline Monte Carlo Statistics.

Parameter	Mean/Median	Deviation	Skewness	Kurtosis
T_c	1255.0/1253.6	38.8	0.25	3.19
T_g	2410.7/2407.4	63.6	0.33	3.29
RN	9589.3/9483.7	1310.7	0.49	3.32

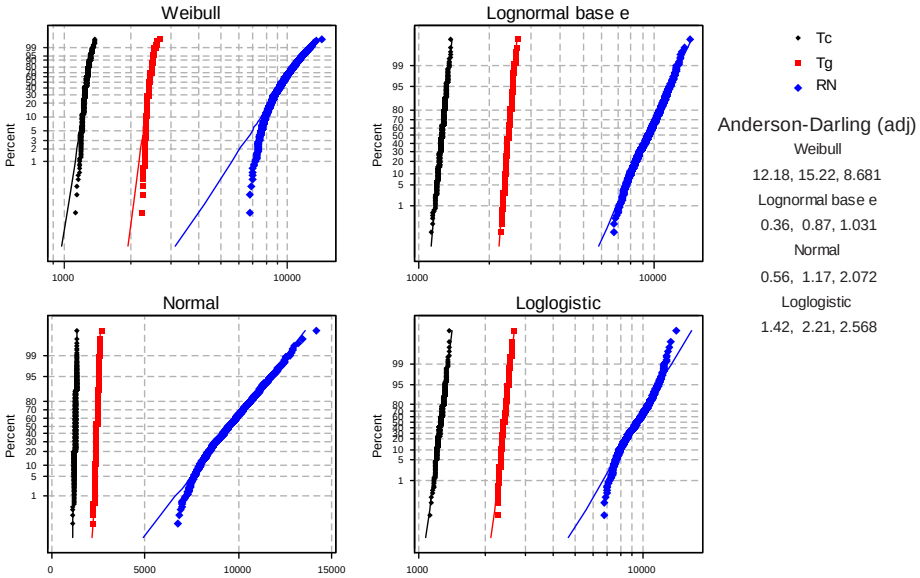

Figure 8. Cycle Response Parametric Distribution Identification

Further statistical analysis of the response parameters indicates the existence of strong positive correlation between all of the parameters. The correlation coefficient matrix for the responses is calculated to be $R = \begin{bmatrix} 1.00 & 0.85 & 0.76 \\ 0.85 & 1.00 & 0.71 \\ 0.76 & 0.71 & 1.00 \end{bmatrix}$. Thus, not only are some of the cycle response parameters non-normal, they are also jointly distributed.

According to the results of the baseline uncertainty assessment, assigning a normal parametric distribution to each of the response parameters and assuming independence would not be statistically justifiable. A solution to this dilemma is given by applying an efficient technique for approximating the response statistics and selecting an appropriate distribution. The adequacy of this technique is assessed using the baseline Monte Carlo statistics.

B. Response Statistics Approximation

As shown by the results of the previous section, assuming that the local component input parameters behave as independent normal random variables would be incorrect. To efficiently quantify this information, a two step technique is demonstrated. First, the response statistics, mean and covariance, are approximated using a sensitivity analysis of the system. Then, a small random sampling of the system is carried out and the proper distributions identified using this sample set.

The response covariances can be approximated as follows. First, define a system of responses each

represented by a linear function of input variables given as

$$\begin{aligned} y_1 &= a_{1o} + \sum_{i=1}^{n} a_{1i} x_i \\ y_2 &= a_{2o} + \sum_{i=1}^{n} a_{2i} x_i \\ &\vdots \\ y_m &= a_{mo} + \sum_{i=1}^{n} a_{mi} x_i \end{aligned} \tag{4}$$

or in matrix form

$$\mathbf{y}_{m\times 1} = \mathbf{M}_{m\times n}\mathbf{x}_{n\times 1}$$

These functions are linear approximations to the actual functional relationships between the cycle response and input parameters. By substituting the approximate functions into the formula for the covariance operator and simplifying, the approximation of the covariance between the i^{th} and j^{th} responses can then be expressed as

$$R_{y_i y_j} = COV(y_i, y_j) \approx \sum_{m=1}^{n}\sum_{l=1}^{n} \frac{\partial y_i}{\partial x_m}\frac{\partial y_j}{\partial x_l} COV(x_m, x_l) \tag{5}$$

where $COV(x_m, x_l)$ is the covariance between the m^{th} and the l^{th} input variables and $\frac{\partial y_i}{\partial x_m}$ is the partial derivative of the i^{th} response with respect to the m^{th} input variable.

Applying equation (5) to the cycle model is relatively straightforward in that only $n+1$ (n perturbation plus 1 mean value cases) cycle model evaluations are required to provide the necessary input to this approach. The choice of the perturbation distance is taken to be $+1\sigma$ for each of the input variables listed in Table 2. Sensitivity derivatives between each response and each of the input parameters can then be computed. Using the sensitivity derivative matrix as input to the covariance approximation formulae the covariance matrix of the response variables is found to be

$$\Sigma = \begin{bmatrix} 1450.0 & 1980.2 & 37720.7 \\ 1980.2 & 3803.3 & 56751.9 \\ 37720.7 & 56751.9 & 1687572.8 \end{bmatrix} \tag{6}$$

and the corresponding correlation coefficient matrix of $R = \begin{bmatrix} 1.00 & 0.84 & 0.76 \\ 0.84 & 1.00 & 0.71 \\ 0.76 & 0.71 & 1.00 \end{bmatrix}$ which agrees very well with the correlation coefficient matrix computed during the baseline validation analysis of the cycle model. The maximum error is 1% for the correlation between T_c and T_g. The mean vector of the cycle responses is approximated by simply evaluating the cycle model using the mean vector of the input parameters specified in Table 2. Standard deviations are computed using the covariance matrix from equation (6) by computing the square root of the covariance matrix diagonal. Both the mean and standard deviation vectors are reported in Table 5. Not surprisingly, these approximations are reasonable compared to the baseline solution with an average error across all six statistics found to be 1.3% and a maximum error of 3.0% for the gas temperature standard deviation. However, without additional information only simple statistics and normal behavior can be estimated.

Table 5. Engine Cycle Statistics Using Covariance Approximation.

Parameter	Mean (% Error)	Standard Deviation (% Error)
T_c	1248.7 (0.5)	38.1 (1.8)
T_g	2401.4 (0.4)	61.7 (3.0)
RN	9474.3 (1.2)	1299.1 (0.9)

To complete this step, the response parameter distributions are identified using an empirical technique based on small sample statistics. A small number of cases is executed using a matrix of randomly generated input cycle input parameter values. Choosing the number of cases is arbitrary. Statistically, the chance of

finding the proper distribution is increased with an increasing number of cases yet a minimum number of cases is strongly desired for efficiency as compared to alternative methods. Already, $n + 1 = 9$ cases were required to approximate the mean and covariance statistics. Therefore, as a rule of thumb $2n = 16$ random cases are then executed for a total of 25 cases.[e]

The probability plots and corresponding Anderson-Darling test statistics for each response using the small-sample randomly generated cases are shown in Figure 9. Using a limited number of randomly generated cases one can demonstrate that the lognormal distribution function is the most appropriate for the cycle analysis response variables as it had the lowest A-D test statistics for each response. Thus, even with additional randomly generated cases the covariance approximation approach for this problem very efficient.

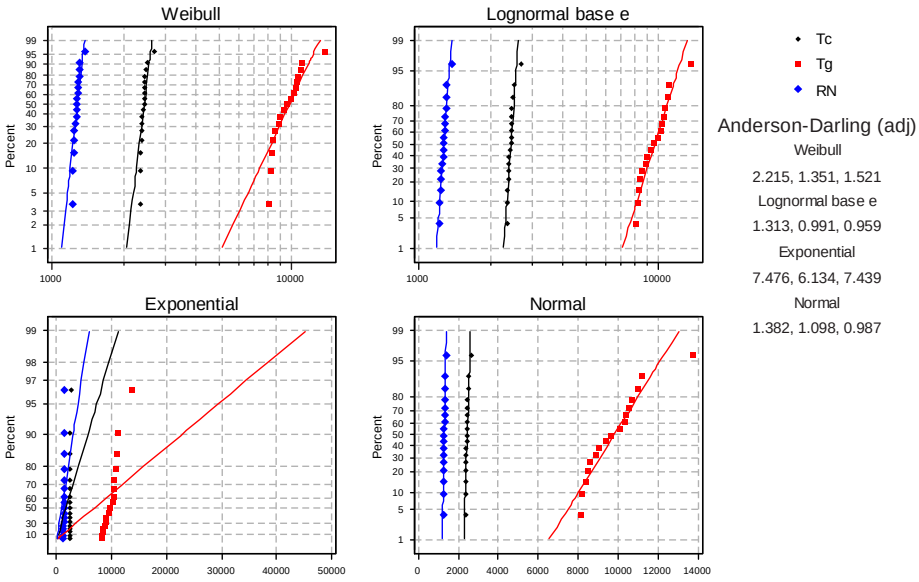

Figure 9. Small Sample Cycle Response Parametric Distribution Identification

Using the small sample statistical results, it was decided to model the cycle responses as lognormal random variables with the mean and variance specified using the values computed using the covariance approximation formula. This lognormal joint distribution space can be validated by computing the marginal distribution statistics and comparing them to the baseline cycle model assessment. The corresponding estimated variable statistics are given in Table 6 showing that the maximum error using this hybrid approach is now only 0.3% which will result in a significant improvement in the accuracy of the input required for a probabilistic analysis of the blade. Also, this additional step is quite interesting in that it allows for a linear statistical approximation method to provide non-normal, even asymmetric statistical information.

Table 6. Engine Cycle Statistics Using Covariance Approximation and Distribution Identification.

Parameter	Mean (% Error)	Standard Deviation (% Error)
T_c	1255.0 (0.0)	38.7 (0.3)
T_g	2410.8 (0.0)	63.5 (0.1)
RN	9587.6 (0.0)	1313.1 (0.2)

[e]This rule of thumb value has additional relevance as the second order approach would require, as a minimum, $2n$ cases and an adequate design of experiments would require 84 cases.

VI. Conclusion

A multi-step approach to creating an appropriate starting point for the probabilistic assessment of components operating in a system was given and demonstrated for a gas turbine blade example. A decomposition of the blade characteristics was conducted with the system safety criteria as guidance. The information organized during this step proved helpful in creating an appropriate modeling and simulation environment for the blade during the synthesis step. Finally, the system's statistical influence on was characterized and quantified using a combination of analytical and small sample empirical statistics which proved to be very accurate and required only a few samples of the overall system analysis. The result of this characterization demonstrated that, at least for this application, the component input parameters should not be modeled by independent, normal random variables which a popular assumption used in component reliability studies.

References

[1]Wallace, J.M., L. Z. W. R. V. V. and Mavris, D., "Annual Progress Report: Probabilistic Life Assessments of Hot Gas Path Components," Internal technical report, General Electric Power Systems, Greenville, SC, May 2002.

[2]Wallace, J. and Mavris, D., "Creep Life Uncertainty Assessment of a Gas Turbine Airfoil," *AIAA2003-1484, 5th AIAA Non-Deterministic Approaches Forum*, Norfolk, VA, April 7-10, 2003.

[3]Wallace, J.M., W. S. and Mavris, D., "Robust Design of a Creep Limited Gas Turbine Component Using the Taguchi Approach," *GT2003-38546, ASME Turbo Exposition*, June 16-19 2003.

[4]"NASA CFM56 Thermodynamic 1-D Cycle Model," NASA Glenn, September 2000.

[5]"Navy/NASA Engine Program (NNEP89): A User's Manual," August 1991.

[6]"Nimonic Alloy 80A," Online technical report (july 2003), Special Metals, www.specialtymetals.com.

[7]Sues, R.H., C. M. P. S. and Wu, J. Y.-T., "Reliability-Based Optimization Considering Manufacturing and Operational Uncertainties," *Journal of Aerospace Engineering*, Vol. 14, No. 4, October 2001, pp. 166–174.

[8]Wallace, J. and Mavris, D., "Propulsion System Reliability Prediction and Optimization Using a Multi-Physics Environment," *AIAA 2002-5561, 9th AIAA/ISSMO Symposium on Multidisciplinary Analysis and Optimization*, Atlanta, GA, September 4–6 2002.

[9]Wu, Y.-T., "An Adaptive Importance Sampling Method for Structural System Reliability Analysis," *Reliability Technology*, Vol. 28, 1992, pp. 217–231.

[10]Pascual, F. and Meeker, W., "Estimating Fatigue Curves with the Random Fatigue Limit Model," *Technometrics*, Vol. 41, November 1999, pp. 277–302.

[11]Orr, R.L., S.-O. and Dorn, J., "Correlations of Creep Rupture Data for Metals at Elevated Temperatures," *Trans. ASM*, Vol. 46, 1954, pp. 113–124.

[12]Daleo, J.A., E.-K. and Woodford, D., "Application of Stress Relaxation Testing in Metallurgical Life Assessment Evaluations of GTD111 Alloy Turbine Buckets," *Journal of Engineering for Gas Turbines and Power*, Vol. 121, January 1999, pp. 129–137.

[13]Daleo, J. and Wilson, J., "GTD111 Alloy Material Study," *Journal of Engineering for Gas Turbines and Power*, Vol. 120, January 1999, pp. 375–382.

[14]Basquin, O., "The Exponential Law of Endurance Tests," *Proceedings of the American Society for Testing and Materials*, Vol. 10, 1910, pp. 625–630.

[15]Dowling, N., *Mechanical Behavior of Materials*, Prentice-Hall, Inc., Upper Saddle River, NJ, 1993.

[16]Jarque, C. and Bera, A. K., "A Test for Normality of Observations and Regression," *International Statistical Review*, Vol. 55, pp. 163–172.